YEAR 1 FINAL REPORT

NASA ITM SR&T award NASW-5006

THERMOSPHERIC O/N_2 BASED ON DE-1 FUV DAYGLOW IMAGING DATA

Douglas J. Strickland (PI), Robin J. Cox, and T. Majeed

Computational Physics, Inc.
2750 Prosperity Ave., Suite 600
Fairfax, VA 22031
703-204-1301

Through June, 1996

1. INTRODUCTION

This report discusses work performed during the second half of Year 1 on Contract No. NASW-5006. The primary objective of the work is to derive global dayside thermospheric O concentrations from DE-1 far ultraviolet imaging data which we are considering under both magnetically quiet and disturbed times. Work to date has been more qualitative in producing maps showing intensity variations beyond those that can be explained by changes in solar zenith angle (SZA) and look angle across an image (Craven et al., 1995; Meier et al., 1994; Gladstone, 1994). In meeting our primary objective, four tasks have been addressed during the reporting period:

1. Investigating the uniqueness of the relationship between the dayglow emission seen using DE-1's 123 filter (dominated by OI 130.4 nm emission) and the column abundance of O relative to N_2 referenced to an N_2 depth of 10^{17} cm^2 (see Strickland et al., 1995 for a discussion of this approach to quantifying thermospheric dayside O concentrations)
2. Completion of the algorithm for rapid conversion of DE-1 disk dayglow measurements to O/N_2 values
3. Applying the algorithm to a simulation in which a model DE image was constructed using TIGCM atmospheres. The retrieved image of O/N_2 was compared to TIGCM O/N_2 obtained by integrations of the TIGCM densities
4. Applying the algorithm to selected DE-1 data.

The next section presents our results from these tasks.

2. RESULTS

2.1 Uniqueness study

We followed an approach similar to that described in the publication of Strickland et al. (1995) which addressed the uniqueness of O/N_2 derived from disk dayglow observations of the ratio of OI 135.6 nm to N_2 LBH intensities. There, a close relationship was observed with an uncertainty of only a few percent between 135.6/LBH and O/N_2. The N_2 reference depth at which the smallest uncertainty exists is ~10^{17} cm^2 which is in the vicinity of 135 km. For DE observations, a greater uncertainty is expected since the relationship of the data to O/N_2 is less direct given that there are no coincident LBH data for forming an O/N_2 intensity ratio. This is the most desirable form of the data for deriving O/N_2 since O is competing with N_2 for the energy of photoelectrons. Greater uncertainty will also arise from the complicated nature of the OI 130.4 nm feature which is produced by more than just photoelectron impact excitation, unlike OI 135.6 nm. The second source is by resonance scattering of solar 130.4 nm photons for which there is no competition with N_2.

To address the uniqueness issue, we used approximately 400 TIGCM atmospheres (R. Roble, personal communication, 1992) simulating disturbed conditions on 3/22/79 at 09:00 UT. The atmospheres refer to locations spanning the full range of longitudes and the partial range of latitudes from 60°N to 60°S. Spectral radiances spanning the range of sensitivity of the 123 filter (~123 to 180 nm) were calculated for an SZA of 60° and for nadir viewing. The calculations were performed with the AURIC model (Strickland et al., 1996). A Hinteregger solar EUV flux was used based on $F_{10.7}$ and $<F_{10.7}>$ values of 184.5 and 182, respectively. Key computational steps include generation of photoelectron fluxes, volume emission rates for OI 130.4 nm, OI 135.6 nm, N_2 LBH, and NI 149.3 nm, and corresponding column emission rates. Multiple scattering effects as well as a description of the 130.4 nm solar resonance source are provided by the REDISTER code of Gladstone (1982; 1988). The calculated spectral radiances were converted to counts using the 123 filter response function (see Fig. 1 in Meier et al., 1995). Figure 1 shows the results displayed in the form of O/N_2 versus the calculated counts for the above set of atmospheres. Each O/N_2 value was obtained by integrating the O and N_2 density profiles within that model atmosphere down to the N_2 reference depth of 10^{17} cm^{-2} and then taking their ratio. The scatter gives an illustration of the degree of uniqueness between counts and O/N_2. The distribution is not as tight as observed by Strickland et al. (1995) for 135.6/LBH (see Fig. 9 in that paper). Our interest is in a given vertical cut through the distribution of points in Figure 1 which shows the spread in O/N_2 for a given simulated measurement. The approximate spread in O/N_2 is ~15%. It should be kept in mind that the spread is specific to a given set of atmospheres and may show modest variation from set to set.

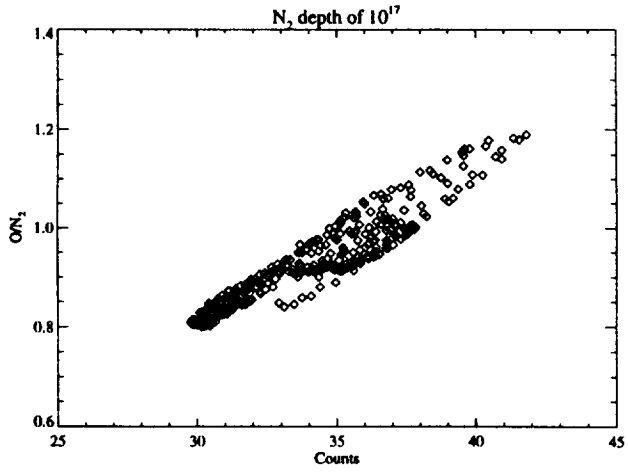

Figure 1. Scatter plot illustrating degree of uniqueness between O/N_2 and modeled FUV dayglow as would be observed by the DE-1 FUV imager using its "123" filter. The modeled dayglow contains OI 130.4 nm, OI 135.6 nm, and N_2 LBH components. Calculations were performed with the AURIC model for an SZA of 60° and for nadir viewing. Approximately 400 TIGCM atmospheres were used to produce the scatter plot. For a given value in counts, the spread in O/N_2 is from ~5 to 15%.

A second exercise carried out to address uniqueness was to scale the O density profiles in our given set of atmospheres so that the radiance calculations for all atmospheres gave the same value for counts. We then examined the dependence of O/N_2 versus the N_2 column density. Figure 2 shows the dependence which may be compared to a similar plot (Fig. 7) in Strickland et al. (1995) where the O density profiles in that set of TIGCM atmospheres were scaled to give the same 135.6/LBH. In that case, all curves gave essentially the same O/N_2 at an N_2 value of 10^{17} cm^{-2}. Here, the spread is considerably greater with no appreciable convergence in the vicinity of 10^{17} cm^{-2}. The uncertainty in O/N_2 as derived from a given value in counts is similar whether the selected reference depth is 10^{17} cm^{-2} or some other nearby value such as 10^{18} or 10^{16} cm^{-2}. Figure 3 shows the distribution of O/N_2 values from Figure 2 at the reference depth of 10^{17} cm^{-2}. Most of the points lie within ±3% of the most probable value although there is a weak bi-modal behavior with several points lying 10% away from this value. Again, we must keep in mind that other distributions can be expected for other choices of model atmospheres. Nevertheless, we expect that the overall behavior displayed in Figure 3 will be similar for other distributions, namely, that most points will lie within a few percent of the most probable value. Distributions like that in Figure 3 were included in the paper by Strickland et al. At the reference depth of 10^{17} cm^{-2}, all points were situated within ±0.5% of the peak value. Even though a greater uncertainty (from a uniqueness perspective) must be assigned to an O/N_2 value derived from counts compared to 135.6/LBH, nevertheless, the magnitude of the uncertainty will not have a significant impact on actual data analysis since a greater uncertainty is expected from systematic and statistical errors in the measurements, themselves.

2.2 Algorithm for mapping counts to O/N_2 values

We have developed an efficient algorithm for mapping an entire DE image of disk dayglow data to a corresponding image of O/N_2. For a given DE image, several simulated images are produced for spherically stratified model atmospheres whose only differences are their O/N_2 values which are intended to span the likely range to be encountered from quiet to disturbed conditions. Within any one of these images, each pixel has been converted from spectral radiance to counts using the 123 filter response function. A way to visualize the full set of simulated results is as a stack of images in which, at a given pixel position, one can move up or down through the stack and observe a monotonic variation in simulated counts that reflects a similar variation in O/N_2. Figure 4 shows an example of this variation for a single pixel associated with a data image to be introduced below. Counts are displayed versus O/N_2. The points displayed on the curve show the O/N_2 values associated with the stack of model images. Such a curve exists for each pixel which has its own SZA and look angle. An interpolation is performed to yield an O/N_2 value for the observed pixel brightness. It should be noted that the mapping is performed *using smooth curves* like that in Figure 3 in spite of the fact that such curves are idealizations of the true relationships between counts and O/N_2. We assume that the curve gives the most likely value of O/N_2 for a given value in counts. Our way of

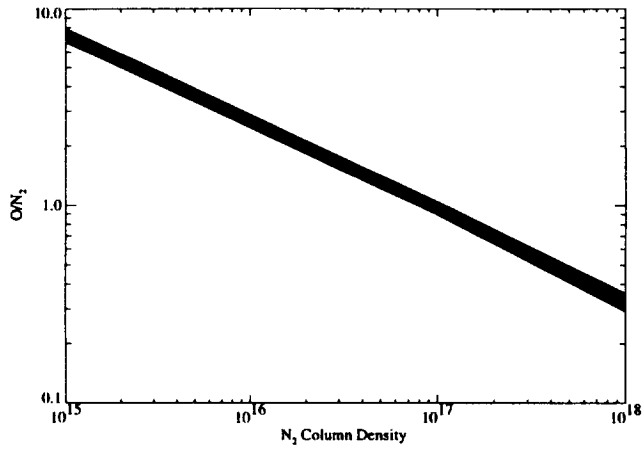

Figure 2. Overplot of curves of O/N_2 versus the N_2 column density for the TIGCM atmospheres used to produce the scatter plot in Figure 1 except for scalings of their O density profiles so that all atmospheres give the same value in counts (35 counts). The results show that there is always a spread in O/N_2 of at least ~15% and that there is little change in its magnitude as a function of N_2 over the range considered. More quantitative information on the spread is given in Figure 3.

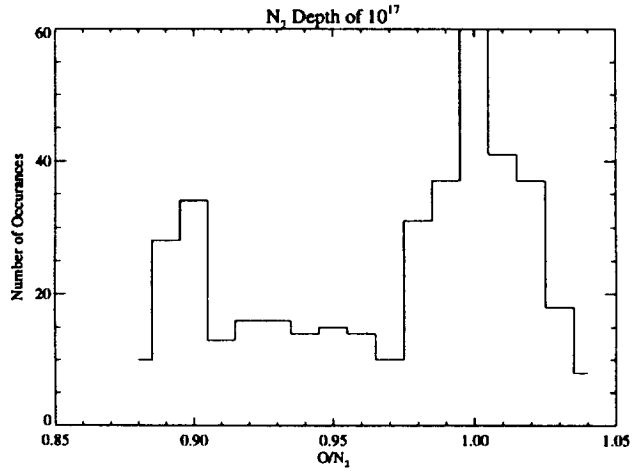

Figure 3. Vertical cut through the overplotted curves in Figure 2 at the N_2 depth of 10^{17} cm^{-2}. Most of the O/N_2 values are within ±3% of the most probable value although several values lie beyond this range with deviations up to10% from the most probable value.

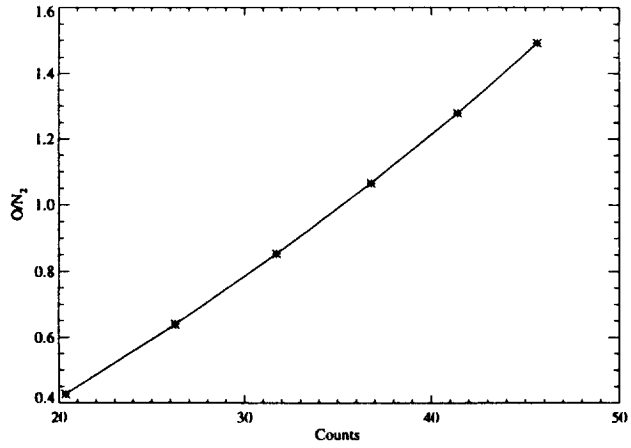

Figure 4. Example of O/N_2 versus counts obtained by scaling the O density profile in an MSIS model atmosphere. The curve illustrates the dependence as seen at a given pixel position within the stack of MSIS-based images used to map DE data to O/N_2 values. Each image in the stack is calculated for a single atmosphere with a given scaling of the O density profile. As one moves through the stack at a given pixel position, the counts change in response to changes in the O scaling factor.

handling the fact that a distribution of O/N_2 values should be assigned rather than a single value is through an error analysis after the mapping that includes errors associated with non-uniqueness along with measurement errors.

The key to fast generation of a given model image is the use of a single model atmosphere for that image. We are currently using MSIS-91 (Hedin, 1991) although the choice in not critical based on the study discussed in 2.1. For a given model atmosphere, spectral radiances containing OI 130.4 nm, OI 135.6 nm, N_2 LBH, and NI 149.3 nm are calculated for the necessary range of look angles and for SZA*s* from 0° to 90°. The radiances are then converted to counts. A simulated image is then rapidly constructed by two dimensional interpolations using paired values of SZA and look angle for each pixel in the selected DE-1 image. The above process is repeated several times for scalings of the MSIS O density profile from a minimum value in the vicinity of 0.25 to a maximum value of about 1.5. O/N_2 at the selected N_2 reference depth (10^{17} cm^{-2}) is calculated for the unscaled atmosphere. The values for the scaled atmospheres relate trivially to the calculated value through the scaling factors.

While the choice of model atmosphere is not critical to constructing the pixel dependent curves of counts versus O/N_2 (by scaling the O density profile several times), the choice of the model solar EUV flux is important since it affects the overall magnitude of these curves. One hopes that the model flux is close to the true flux at the time of the

observation given the further qualification that the data are well calibrated. There will be some bias between the measured counts (ignoring for the moment statistical errors) and the corresponding curve of counts versus O/N_2 due to some degree of inconsistency between the model flux and actual flux coupled with any inconsistency between the actual flux and measured counts due to calibration errors. The bias in turn will lead to a bias in the overall magnitude of O/N_2 across the image but will not significantly effect relative variations. Our approach to investigating this bias is to compare a model image to data during geomagnetically quite times for which it is expected that a model like MSIS gives an O/N_2 value close to the actual average value over the dayside region being observed. Any bias between the images is then interpreted in terms of an inconsistency between the model solar EUV flux and the observations which is then removed by scaling the model flux.

Our primary interest in using the algorithm being discussed is to derive O/N_2 maps from a sequence of images during storm periods. For such a given period (usually one to two days), the model solar EUV flux is specified using $F_{10.7}$ and $\langle F_{10.7} \rangle$ values from a time just prior to this period. The above procedure is then used to remove any bias by scaling the solar flux. In the application to follow, a reduction by 22% was required to remove the bias. We assume that no changes occur in the actual solar flux over the brief period of interest. It is possible to vary the model flux during this period which would be reflected through changes in the magnitudes of the many curves of model counts versus O/N_2 used to convert the data. This would only be done if a significant change in $F_{10.7}$ occurred during the storm period. Significant changes do not usually occur over such short time intervals. Furthermore, $F_{10.7}$ is given as a daily value which does not give the needed time resolution for considering changes to the model flux in addressing the several images recorded during a given day. Our approach at this time is to assume that the actual flux does not change during a given storm period.

2.3 Testing the algorithm on a simulated DE image based on TIGCM atmospheres

The NCAR TIGCM calculates 3D thermospheric densities on a global scale. We have used these densities for a particular date and time to simulate a DE image. The model densities and data do not refer to the same date and time which is not important to the simulation. Figure 5 shows the simulated image in the lower half of the display. The image in the upper half was obtained for a single MSIS model atmosphere. The simulations were done for a DE image obtained on July 13, 1982 at 23:21 UT (the actual data will be presented in 2.4). The computing times needed to generate the MSIS- and TIGCM-based images were ~20 s and ~6 hrs, respectively. Times refer to an SGI Iris Indigo R4000 system. Much more time was needed for producing the TIGCM-based image since spectral radiances were calculated for a large set of atmospheres in contrast to calculations for a single atmosphere in the case of the MSIS-based image. The differences between the images in Figure 5 due to atmospheric effects are masked by the

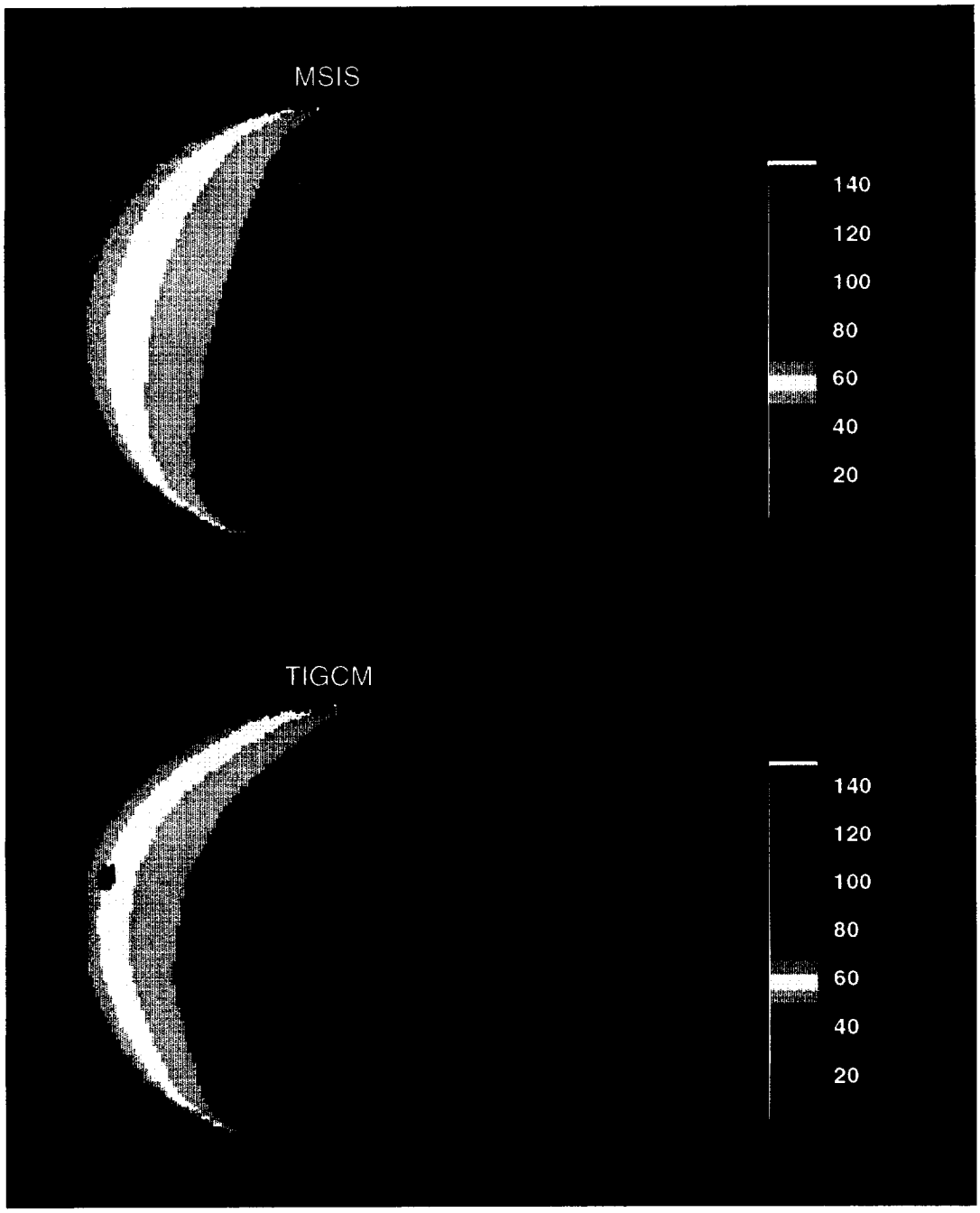

Figure 5. Two simulations of a DE image obtained on July 13, 1982 starting at 23:21 UT. The units are counts for the "123" filter. The top image was obtained for a single MSIS atmosphere. The bottom image was obtained for a non-spherical distribution of densities from NCAR's TIGCM.

variations across the images due to changing SZA and look angle. These effects are removed by taking the ratio of images which is displayed in the upper part of Figure 6. We refer to such an image as rectified meaning that SZA and look angle effects have been removed. The numerator contains the TIGCM image. One can infer from the color table that less O is present for TIGCM in the central region of the image but then becomes greater than MSIS as one moves north and south away from this region. The middle image displays O/N_2 derived from the TIGCM image in Figure 5 using the algorithm from 2.2. The structure is similar to that in the rectified image. The true TIGCM O/N_2 is displayed in the third image in Figure 6. The true values were obtained by integrating the O and N_2 density profiles in the full set of TIGCM atmospheres down to the reference depth of 10^{17} cm^{-2}. We observe agreement between derived and true to better than 90% over most of the image which is consistent with the degree of uniqueness between counts and O/N_2 for TIGCM atmospheres.

2.4 Applying the algorithm to selected DE-1 data

O/N_2 has been derived from two DE images recorded during a major geomagnetic storm that occurred on July 12 - 15 (Days 193 - 196), 1982. Preliminary analysis of several images during this storm was reported by Meier et al. (1994) in a report documenting work during the third year of NASA Contract S-42047-E. The work was a joint effort by NRL and CPI and led to rectified images and comparisons in structure within these images to TIGCM structure for the same storm period. The data to be considered were obtained on July 13 (Day 194) starting at 23:21 UT (approximately eleven minutes is required to record an entire image) and on the following day starting at 12:41 UT. Figure 7 shows A_p during these two days and reflects very disturbed conditions at the end of July 13. A quiet-time image from July 13 (measurement started at 14:54 UT) was used to examine the degree of bias between the data and model. The Hinteregger solar EUV flux was based on $F_{10.7}$ and $\langle F_{10.7} \rangle$ values appropriate to that date (252.6 and 174.9, respectively). The rectified image obtained by dividing the data by the simulated image shows a bias of ~22% when displayed as a distribution of pixel occurrences versus the ratio of observed to simulated counts. The bias was removed by reducing the Hinteregger flux by this same percentage. The adjusted distribution is shown in Figure 8. The degree of symmetry suggests that statistical fluctuations in the data are primarily responsible for the spread. Deviations from spherical symmetry in the actual atmosphere will also contribute to the spread since the model image is based on a single MSIS atmosphere. Such details are not important with regard to this quite-time distribution since its only purpose is to correct any obvious bias between the data and model prior to examining the behavior of O during storm conditions.

Having adjusted the model solar EUV flux, we now turn our attention to the first of the two selected times during the July, 1982 storm. The data appear in the upper portion of Figure 9 followed by their rectification (middle portion) and the derived O/N_2 (lower portion). O depletions are visible in each of the images, although more difficult to

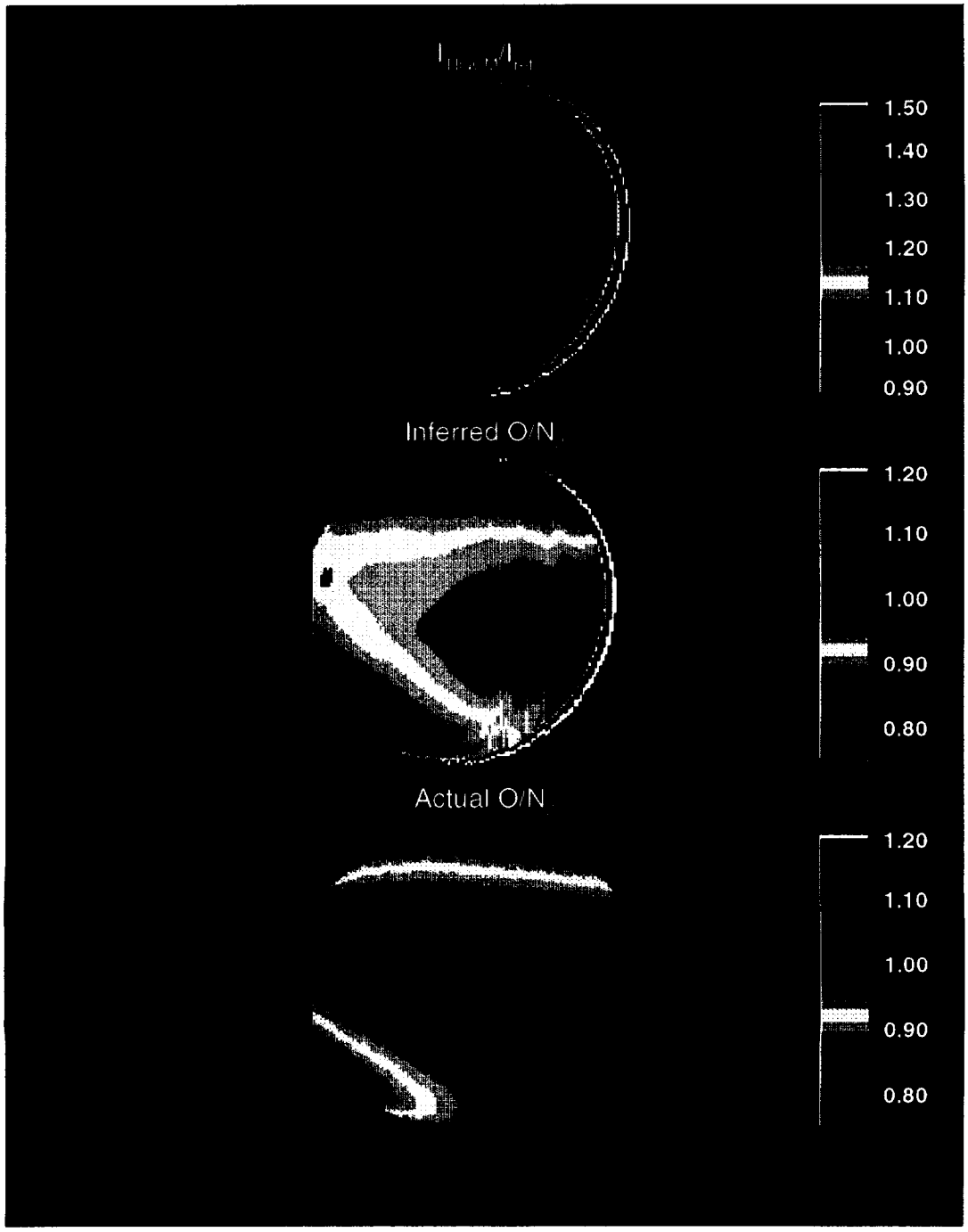

Figure 6. Ratio of images from Figure 5 (top), inferred O/N_2 from the bottom image in Figure 5 using a stack of corresponding MSIS-based images (middle), and the "actual" O/N_2 obtained by integrating TIGCM density profiles down to the N_2 reference depth of 10^{17} cm^{-2}. The inferred values are typically within 10% of the "actual" ones.

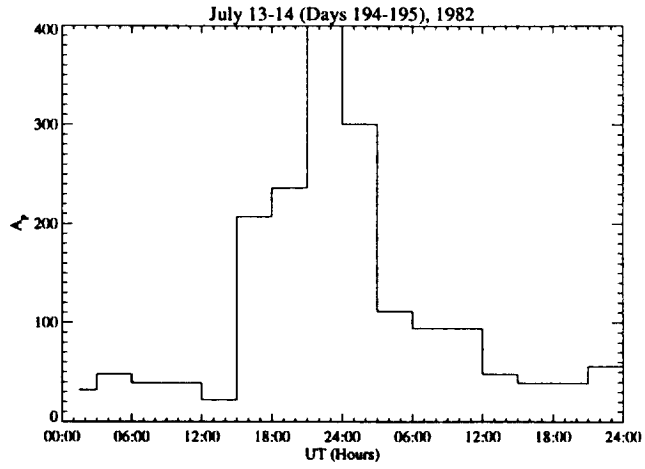

Figure 7. The geomagnetic index A_p over the 48 hour period on July 13 and 14, 1982. The DE data to follow were recorded during hour 23 UT on July 13 and during hour 12 UT on July 14.

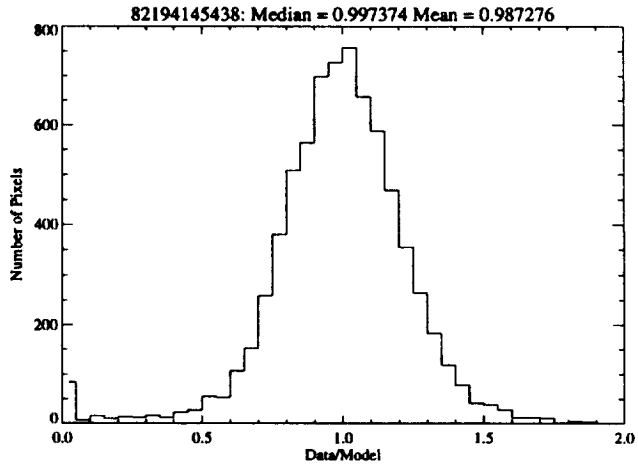

Figure 8. Distribution of pixel occurrences versus the ratio of observed to simulated counts from a quiet-time rectified image just prior to the onset of the July, 1982 geomagnetic storm. The starting time for recording the image was 14:54 UT on July 13. The Hinteregger solar EUV flux was decreased by 22% in order to produce this unbiased distribution.

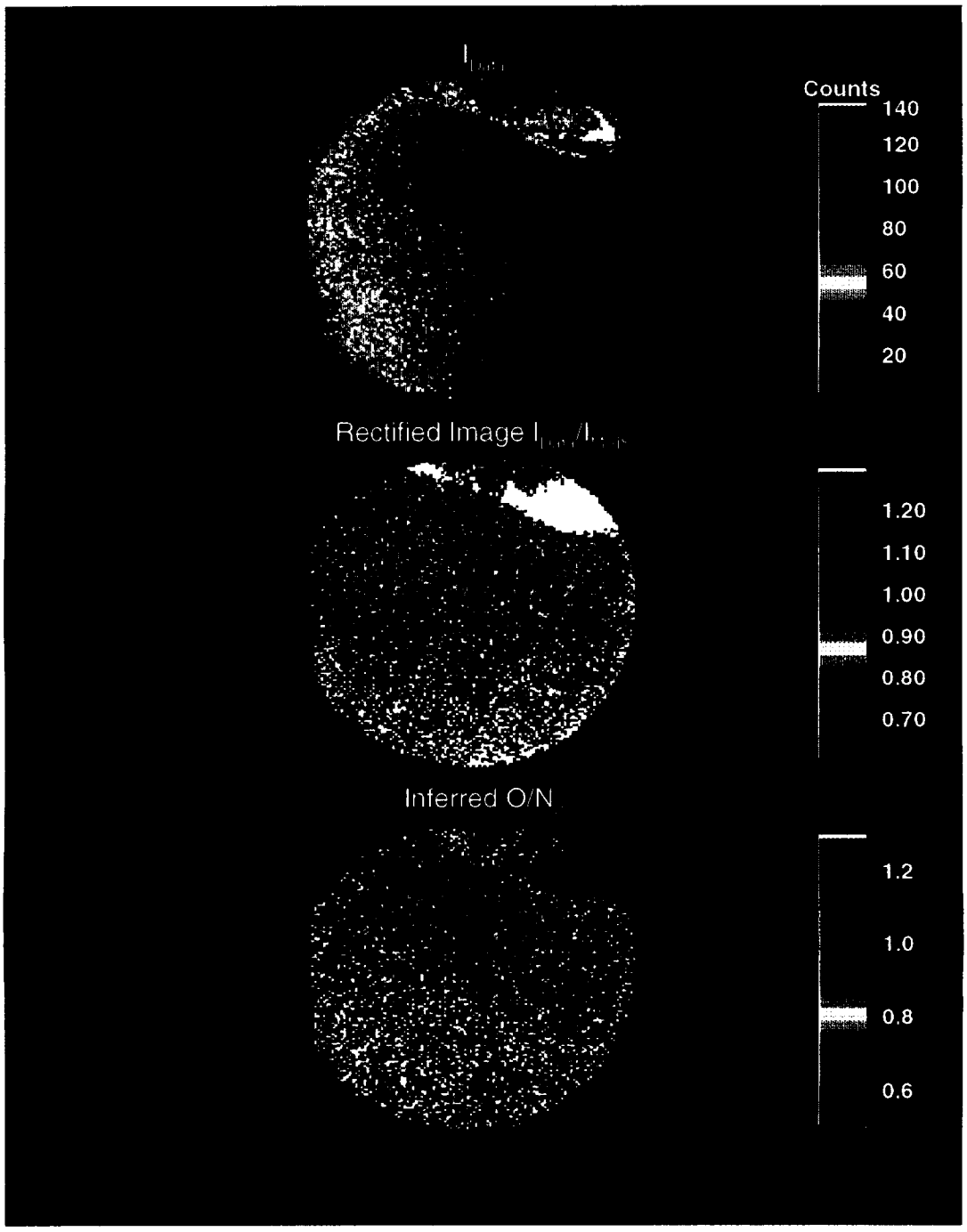

Figure 9. DE image recorded during hour 23 UT on July 13 (top), its rectification (middle) obtained by dividing the image by an MSIS-based simulation, and inferred O/N_2 (bottom).

see in the unrectified data. The rectified image is not used to derive O/N_2 but serves to illustrate that thermospheric structure can be seen much better in the data following the removal of SZA and look angle effects. The simulated image used to rectify the data is based on the same solar EUV flux and MSIS atmosphere used in the pre-storm rectification that produced the distribution in Figure 8. The high latitude portions of the rectified and O/N_2 images should be ignored since they are contaminated by auroral emissions. The O/N_2 image shows a large area containing values less than unity below the auroral oval in the northern hemisphere extending to low latitudes. By contrast, the above MSIS model atmosphere possesses an O/N_2 value of .99 (at the N_2 reference depth of 10^{17} cm^{-2}). Thus, we may refer to the region just discussed as one containing O depletions relative to expected quiet time values. No significant depletions appear in the portion of southern hemisphere seen in the image. Figure 10 shows the latitudinal variation of O/N_2 through a vertical swath in the center of the image that is five pixels wide. The smooth curve was obtained by fitting a polynomial to the derived values. One of the purposes in showing a cut through the image is to better illustrate the noise in the data which is due to low counting statistics. Another is the more quantitative perspective achievable from this type of plot compared to a false color image. It is clear from the scatter that the statistical errors dominate those due to non-uniqueness between a true intensity and O/N_2. The results show a marked asymmetry between the hemispheres with O depletions above the geographic equator exceeding 50%.

The distribution from the rectified image in Figure 9 is shown in Figure 11. It is of interest to compare this with the pre-storm distribution. A shift is seen to the left and the distribution is less symmetric with a slower decrease to the right of the peak. The shift serves as another indicator of the decrease in O relative to pre-storm values.

The second image to be addressed was recorded approximately thirteen hours after the one discussed above starting at 12:41 UT. Figure 7 shows that A_p was in rapid decline from the extreme value of ~400 at 00:00 UT to ~100 at 12:41 UT. Figure 12 shows the data, its rectification, and O/N_2 similar to Figure 9 for the first data set. The rectified image and the O/N_2 image show a somewhat uniform region of depletion in longitude above the equator. Figure 13 shows a vertical cut though the O/N_2 image similar to the cut shown in Figure 10 from the first data set. The depletion pattern is similar but more O is present below 15° N. Enhancements in O at low latitudes during disturbed times were also observed by Strickland and Thomas (1976) using zenith viewing OI 130.4 nm dayglow observed from the OGO-6 satellite. The distribution from the rectified image in Figure 12 appears in Figure 14. The pattern is similar to that in Figure 11 with a modest increase in asymmetry most noticeably to the right of the peak. This reflects the many pixels at low latitudes in which there appear to be O enhancements.

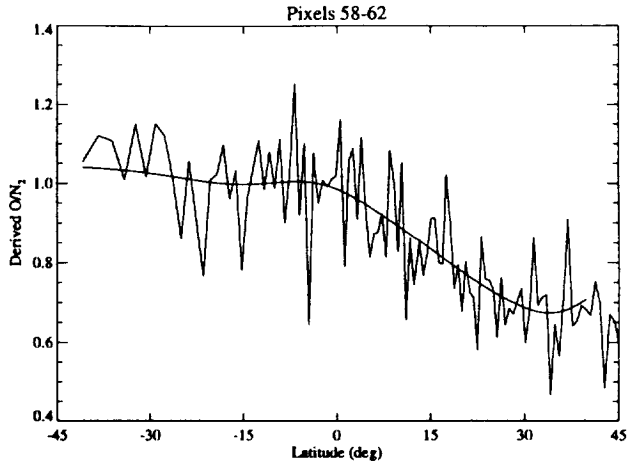

Figure 10. Five pixel-wide vertical cut through center of O/N_2 image from previous figure. The smooth curve is a fit to the results which contain noticeable fluctuations due to low counting statistics.

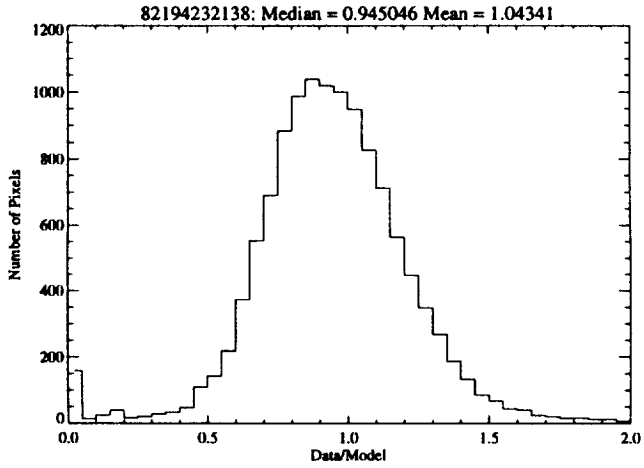

Figure 11. Distribution of ratio values from the rectified image in Figure 9. This distribution is more asymmetric than the pre-storm distribution in Figure 8 and is shifted to the left. The shift serves as another indicator that less O is present than just before the storm provided the solar EUV flux has not decreased from it pre-storm magnitude.

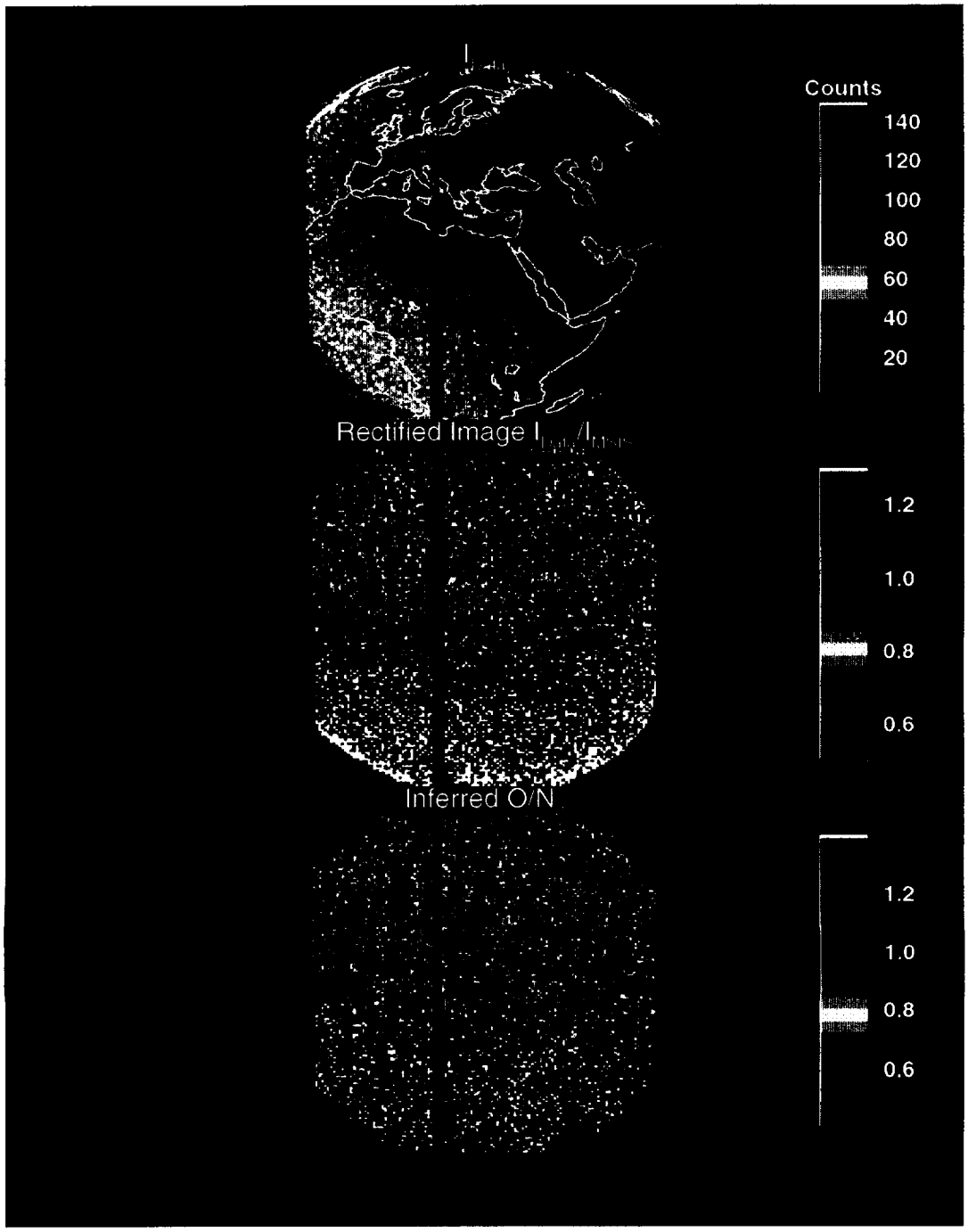

Figure 12. Similar to Figure 9 except approximately 12 hours later.

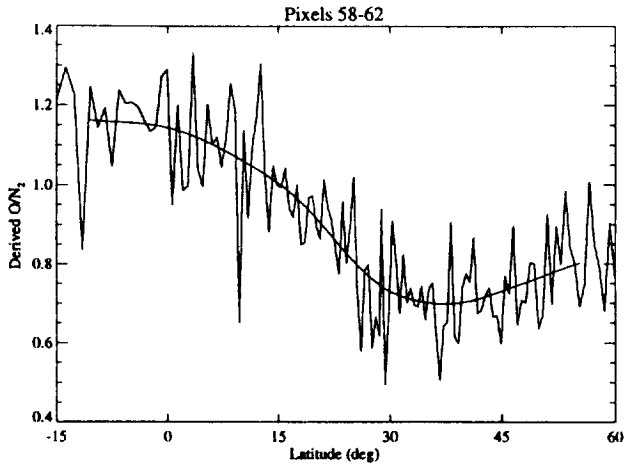

Figure 13. Five pixel-wide vertical cut through center of O/N_2 image from previous figure. These results show a similar pattern of O depletion at northern latitudes seen twelve hours earlier but now more O is present at low latitudes.

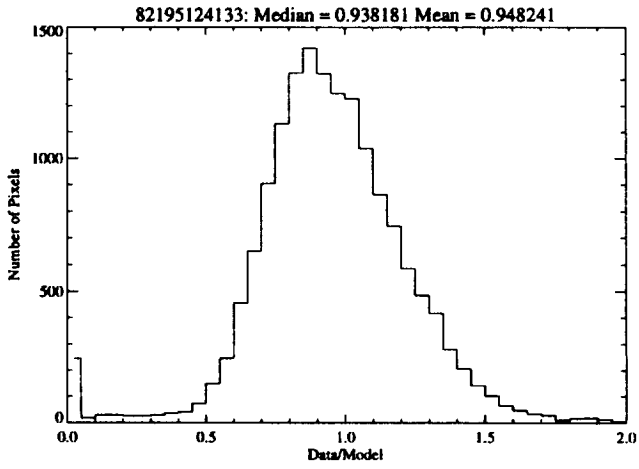

Figure 14. Distribution of ratio values from the rectified image in Figure 12. The distribution is similar to that in Figure 11 showing a shift to the left but is more asymmetric with a slower decrease to the right of the peak.

3. YEAR 2 INVESTIGATIONS

Two papers to be submitted to JGR are being written describing the above work. The first will be based on the contents of this report . The second paper will examine the evolution of O/N_2 during the July, 1982 storm, relate the results to TIGCM predictions, and also relate the results to what is known about the energetics of the storm based on DE images of the aurora, magnetometer data, and possibly other relevant data sets.

There will be analysis of DE data from at least one other storm period. We also propose to examine selected UVI data from the POLAR experiment given that superior global descriptions of O/N_2 should be achievable. Near simultaneous "multi-color" FUV images are being obtained for much shorter integration times. It should be possible to produce images of ratios of 135.6 nm to LBH intensities which have a less ambiguous relationship to O/N_2 compared to DE 123 filter data. Issues such as changes in solar EUV and calibration are unimportant for deriving O/N_2 from data ratios.

REFERENCES

Craven, J. D., A. C. Nicholas, L. A. Frank, and D. J. Strickland, Variations in FUV dayglow brightness following intense auroral activity, *Geophys. Res. Lett.*, *21*, 2793, 1994.

Gladstone, G. R., Radiative transfer with partial frequency redistribution in inhomogeneous atmospheres: Application to the Jovian aurora, *J. Quant. Spectrosc. Radiat. Transfer, 27*, 545, 1982.

Gladstone, G. R., UV resonance line dayglow emissions on Earth and Jupiter, *J. Geophys. Res., 93*, 14,623, 1988.

Gladstone, G. R., Simulations of DE 1 UV airglow images, *J. Geophys. Res., 99*, 11,441, 1994.

Hedin, A. E., Extension of the MSIS thermosphere model into the middle and lower atmosphere, *J. Geophys. Res., 96*, 1159, 1991.

Meier, R. R., A. Nicholas, R. Cox, and D. J. Strickland, Progress report on third and final year activities - NASA Contract # S-42047-E, September, 1994.

Meier, R. R., R. J. Cox, D. J. Strickland, J. D. Craven, and L. A. Frank, Interpretation of Dynamics Explorer far UV Images of the Quiet Time Thermosphere, *J. Geophys. Res.*, *100*, 5777, 1995.

Strickland, D. J., J. S. Evans, and L. J. Paxton, Satellite remote sensing of thermospheric O/N_2 and solar EUV: 1. Theory, *J. Geophys. Res., 100*, 12,217, 1995.

Strickland, D. J., J. S. Evans, J. E. Bishop, T. Majeed, P. M. Shen, R., and R. E. Huffman, Atmospheric Ultraviolet Radiance Integrated Code (AURIC): Current capabilities for rapidly modeling dayglow from the far UV to the near IR, *SPIE, Ultraviolet Atmospheric and Space Remote Sensing: Methods and Instrumentation*, 1996.

Strickland, D. J., and G. E. Thomas, Global atomic oxygen density derived from 0G0-6 1304-A airglow measurements, *Planet. Space Sci., 24*, 313, 1976.